Materials Research Express

PAPER • **OPEN ACCESS**

Fabrication and characterization of Schottky barrier diodes on rutile TiO_2

To cite this article: Julie Bonkerud *et al* 2020 *Mater. Res. Express* **7** 065903

Materials Research Express

PAPER

Fabrication and characterization of Schottky barrier diodes on rutile TiO_2

Julie Bonkerud[1], **Christian Zimmermann**[1], **Philip Michael Weiser**[1], **Thomas Aarholt**[1], **Espen Førdestrøm Verhoeven**[1], **Lasse Vines**[1], **Eduard V Monakhov**[1] **and Frank Herklotz**[2]

[1] University of Oslo, Physics Department/Centre for Materials Science and Nanotechnology, PO Box 1048 Blindern, Oslo N-0316, Norway

[2] Technische Universität Dresden, Institute of Applied Physics, 01062 Dresden, Germany

E-mail: julie.bonkerud@smn.uio.no

Keywords: Schottky barrier diodes, TiO_2, degradation

OPEN ACCESS

RECEIVED
26 February 2020

REVISED
6 May 2020

ACCEPTED FOR PUBLICATION
28 May 2020

PUBLISHED
10 June 2020

Abstract

Schottky barrier diodes (SBDs) were fabricated by depositing Pd, Pt or Ni on single crystal, conductive *n*-type rutile TiO_2 using e-beam evaporation. As-grown and nominally undoped rutile TiO_2 single crystals are semi-insulating, and were heat-treated in forming gas flow, N_2 flow or H_2 gas to obtain conductive *n*-type crystals displaying electrical conductivities in the range of $(0.5 - 8) \times 10^{-2}\ \Omega^{-1}\ cm^{-1}$. Additionally, SBDs were deposited on Nb-doped conductive *n*-type rutile TiO_2 with a conductivity of around $0.25\ \Omega^{-1}\ cm^{-1}$. Generally, SBDs displaying a rectification of up to eight orders of magnitude were obtained, when comparing the current under reverse and forward bias. The extracted ideality factors were in the range of $1.1 - 4.0$. From Capacitance-Voltage measurements, the built-in voltage was derived to be around 1.2 V–1.9 V, depending on the doping concentration of the specific TiO_2 single crystal. Series resistances as low as 19 Ω were achieved. A considerable variation in the electrical characteristics of different SBDs deposited on the same crystal was found, regardless of the metal or doping strategy used. Moreover, the SBD characteristics change over time, particularly seen as a degradation in rectification, mainly related to an increase in the current under reverse bias. Additional surface treatments such as boiling in H_2O_2 and etching in HF do not have a significant effect on the quality of the SBDs. Clear indications for poor adhesion between TiO_2 and Pd are shown. In conclusion, we demonstrate the fabrication of SBDs which are suitable for studying the fundamental properties of metal/TiO_2 junctions and the characteristics of electrically-active defects in TiO_2 using space-charge spectroscopy.

1. Introduction

Rutile titanium dioxide (TiO_2) is a wide-bandgap semiconductor ($E_g = 3.2$ eV [1–4]) well-known for its photo-catalytic properties [5, 6], rendering TiO_2 a promising material for photo-catalytic water-splitting as well as photo-catalytic water purification [6–10]. Conductive *n*-type TiO_2 is of particular interest for such applications due to its lower resistivity and more pronounced optical absorption in the visible and infrared part of the electromagnetic spectrum compared to pristine TiO_2 [11–14]. It is possible to achieve *n*-type doping in TiO_2 by incorporating Nb [13, 15–17] or by heat-treating TiO_2 in hydrogenating or reducing atmospheres [11, 14, 15, 18–20]. Hydrogenated as well as reduced TiO_2 have been used in photo-catalytic applications [11, 12, 14, 21]. However, there is still no agreement on the nature of the main donors in hydrogenated and/or reduced TiO_2 [22–24]. Defects are also believed to play a role in the optical absorption in the visible and infrared part of the electromagnetic spectrum displayed by conductive *n*-type TiO_2 [14, 25–28]. Thus, understanding the properties of defects in TiO_2 is important to improve photo-catalytic applications involving TiO_2.

In applications for photo-catalysis, systems consisting of TiO_2 and noble metals, such as Pd, Pt, Au or Ag, display a better performance compared to just TiO_2 [29–33]. This is believed to be due to an improved charge

transfer at the interface between the metal and TiO_2 due to the formation of a rectifying junction [34]. Besides photo-catalytic applications, rectifying metal/TiO_2 junctions are also of interest for UV photo-detectors [35], hydrogen sensors [36] and switching devices [37–39].

In order to improve metal/TiO_2 junctions for all applications mentioned above, the charge transfer across the interface needs to be understood better. This requires knowledge regarding the electrical characteristics of rectifying metal/TiO_2 junctions, where simplified model systems are often a superior starting point for such investigations. Besides studying the properties of the metal/TiO_2 junctions themselves, the junctions can also be used to probe the properties of defects in TiO_2 using space-charge spectroscopy [16, 40, 41]. Thus, the fabrication of Schottky barrier diodes (SBDs) involving conductive TiO_2 single crystals obtained by employing different doping strategies paves the way for systematic defect studies in such material as well as enables investigations of the fundamental properties of the corresponding metal/TiO_2 junctions.

SBDs have been achieved on TiO_2 using Pt [42–44], Pd [45–47], Ni [48] and Au [19, 49–51]. The characteristics of these SBDs show a varying degree of non-ideal behaviour. Although there is a considerable amount of literature on SBDs involving TiO_2, only a few reports exist comparing SBDs on differently doped TiO_2 crystals fabricated in the same laboratory. Additionally, there is a general concern about the long-term stability of metal/TiO_2 junctions [42, 46, 52], but the change in electrical characteristics over time has not been addressed in depth. In hydrogenated TiO_2, the incorporated H might affect the SBDs. It has been shown that the current in junctions formed between different metals and *n*-type-type single crystalline TiO_2 is sensitive to hydrogen in the ambient [49], and a reaction between H and Pd may cause SBDs to degrade [46, 47, 49].

In the present work, we have systematically studied the electrical behaviour of junctions formed between Pd, Pt, Ni as well as Al and *n*-type TiO_2 single crystals doped with Nb or doped by heat-treatments in hydrogenating or reducing atmospheres. The concentration of interstitial hydrogen (H_i) in the different types of TiO_2 crystals was measured. The variation in SBD characteristics for diodes deposited on the same TiO_2 crystal was investigated. First, SBD characteristics using different metals are compared. SBDs were obtained for Pd/TiO_2, Pt/TiO_2 and Ni/TiO_2 with up to eight orders of magnitude in rectification. Following this, a comparison of Pd/TiO_2 SBDs using TiO_2 with different dopants and different H_i concentration is presented. The diode characteristics showed a pronounced change over time, related to a decrease in overall rectification. Detailed measurements concerning the degradation are presented. The fabricated Pd/TiO_2 junctions are found to exhibit suitable electrical characteristics for studying fundamental junction properties and the characteristics of electrically-active defects in TiO_2 using space-charge spectroscopy.

2. Experimental

Rutile TiO_2 single crystals with a thickness of 0.5 mm exhibiting different surface orientations grown by the float-zone (FZ) method or the Verneuil (V) method were purchased from *MTI Corporation* [53] and *Shinkosha* [54], respectively. In the following, a TiO_2 crystal with surface orientation (X) is denoted as TiO_2(X). Nominally undoped FZ- and V-grown single crystals were obtained, while V-grown single crystals doped with 0.05wt% of Nb were also acquired. Nominally undoped TiO_2 single crystals were transparent and semi-insulating with a conductivity of $\sigma < 10^{-7}\Omega^{-1}\,\mathrm{cm}^{-1}$. The as-received wafers were cut into pieces measuring approximately $5 \times 5\ \mathrm{mm}^2$ using a laser cutter. After cutting, all crystals were cleaned in an ultrasonic bath with acetone, isopropanol and de-ionized water for 5 min each (standard cleaning procedure).

Afterwards, the undoped samples were exposed to one of the following heat treatments (annealings):

1. Annealing in forming gas (FG) flow ($N_2 + H_2$ with $[H_2]/[N_2] \approx 1/9$) at temperatures between 500 °C and 600 °C. The annealing duration was 35–90 min. After annealing, the samples were cooled-down rapidly in the gas flux.
2. Annealing in closed ampoules filled with approximately 0.5 bar of H_2 gas. The ampoules were evacuated before filling with H_2. These crystals were annealed at temperatures between 400 °C and 600 °C for 10–90 min. After annealing, the crystals stayed in the ampoules during cool-down.
3. Annealing in N_2 flow at temperatures between 980 °C and 1200 °C. The typical annealing duration was in the order of hours (1.25–25 h). After annealing, the samples were taken out of the furnace and the cool-down occurred in N_2 flow.

A tube furnace was used for annealing. All TiO_2 crystals were put into the furnace after the desired annealing temperature was reached. In the following, TiO_2 crystals which have been annealed in FG flow, H_2 gas or N_2 gas are denoted as FG-TiO_2, H_2-TiO_2 and N_2-TiO_2, respectively. Nb-doped crystals are denoted as Nb-TiO_2.

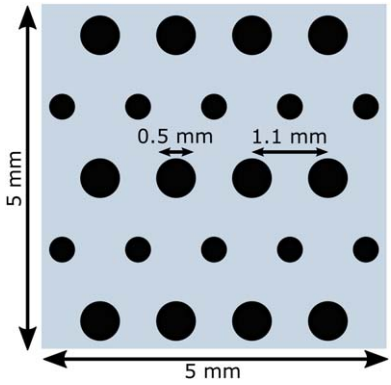

Figure 1. Sample layout showing the front side of a TiO_2 crystal with 22 metal contacts deposited, displaying approximate diode sizes and distances. The crystal is 500 μm thick, and the Ohmic contact is covering the back side of the sample.

Ni, Pd, Pt and Al were deposited onto TiO_2 single crystals subjected to the heat-treatments described above, and Pd was deposited onto Nb-TiO_2 crystals (thickness ~150 nm). Circular metal contacts displaying areas of $(0.67 - 6.36) \times 10^{-3}$ cm^2 were obtained using a shadow mask. Either eutectic InGa was applied to or a stack of Ti/Al was deposited onto the back side of these crystals as Ohmic contacts. All metal depositions were performed using e-beam evaporation. In between depositing or applying metals, the crystals were cleaned using the standard cleaning procedure described above. Typically, between 15 to 20 SBDs are obtained on a piece of TiO_2 crystal (see figure 1 for an overview of the resulting sample layout). Some crystals were subjected to surface treatments prior to the deposition of the circular Ni, Pd, Pt or Al contacts. These crystals were exposed to boiling H_2O_2 for 1–3 min, and some of them were additionally exposed to HF for 5 min. Crystals that were exposed to HF in addition to H_2O_2 will be denoted as TiO_2(X)-HF in the following.

Fourier-Transform infrared spectroscopy (FT-IR) was used to determine the concentration of H_i denoted as [H_i] in TiO_2 single crystals. The investigated TiO_2 single crystals had a surface orientation of (001). Infrared (IR) transmittance spectra were measured using an evacuated Bruker IFS 125HR spectrometer equipped with a globar light source, a KBr beamsplitter, and a liquid-nitrogen-cooled InSb detector. The IR beam was kept at normal incidence ($\pm 3^\circ$) with respect to the (001) surface of the TiO_2 single crystals. Measurements were performed at room temperature using a spectral resolution of 1 cm^{-1}. [H_i] was determined from the integrated area of the optical absorption associated with a local vibrational mode of H_i [55] using a calibration factor determined by Johnson *et al* [56].

The electrical conductivity, σ, and resistivity, ρ, of TiO_2 single crystals was determined using a four-point probe measurement according to the van-der-Pauw method [57, 58]. The measurement utilized a Keithley 7001 switching system, a Keithley 2182A nano-volt-meter and a Keithley 6221 current source. Eutectic InGa pads were used as Ohmic contacts in the corners of the TiO_2 single crystals.

A sample for Scanning Transmission Electron Microscopy (STEM) was prepared by focused ion beam (FIB) using a Ga-ion JEOL JIB-4500. Before milling, a 700 nm W film was deposited in order to protect the underlying sample against Ga damage.

Current-Voltage (IV) measurements were carried out on the metal/TiO_2 junctions under dark conditions at variable temperatures in the range between 25 K and 330 K using a Keithley 6487 unit. Measurements below room temperature were performed in vacuum and within a closed-cycle He cryostat. Capacitance-Voltage (CV) measurements were carried out under dark conditions using an Agilent 4284A LCR meter at six different probing frequencies f_{meas} between 1 kHz and 1 MHz. According to the Mott-Schottky theory of metal-semiconductor junctions, the barrier height, Φ_B, depends on the metal work function, Φ_m, and the semiconductor electron affinity, χ_s; $\Phi_B = \Phi_m - \chi_s$ [59]. Rectifying junctions are formed for $\Phi_B > 0$, while Ohmic contacts are obtained for $\Phi_B < 0$. The expected barrier height Φ_B for SBDs between TiO_2 and Pd, Pt, Ni as well as Al are summarized in table 1. Here, an electron affinity of $\chi_s = 4.33$ eV for TiO_2 was assumed [60]. From IV measurements, the series resistance, R_s, shunt resistance, R_{sh}, ideality factor, η, and average rectification was deduced. η incorporates all the effects that make the device non-ideal [61]. Here, R_s represents the transport of charge carriers through the bulk (on-state resistance) and through the Ohmic contact. ρ_{IV} was calculated from R_s, extracted from IV measurements on SBDs, and sample dimensions; $\rho_{IV} = R_s A/l$. $l = 500$ μm is the crystal thickness, and A is the area of the different SBDs. R_{sh} determines the amount of reverse leakage current. The average rectification of the diodes was calculated by computing the ratio between the average current under reverse and forwards bias. For averaging, the voltage ranges between ± 2 V and ± 4 V for V was chosen. Diodes that showed a rectification lower than one order of magnitude after contact deposition

Table 1. Metal work functions and expected barrier heights Φ_B for metal/TiO_2 junctions, assuming $\chi_{TiO_2} = 4.33$ eV [60]. Rectifying junctions are expected for Pd, Pt and Ni, while for Al, Ohmic contacts are expected.

Metal	Metal work function [64] Φ_m (eV)	Expected barrier height Φ_B (eV)
Pd	5.12	0.8
Pt	5.65	1.3
Ni	5.15	0.8
Al	4.28	—

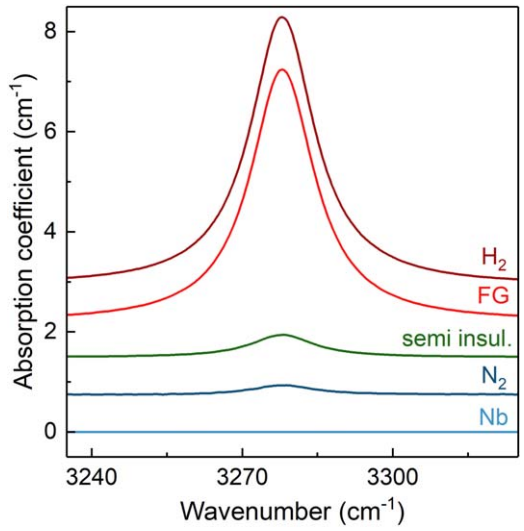

Figure 2. Infrared absorption spectra of the 3278 cm^{-1} H_i vibrational line for as-received samples (semi insulating and Nb-doped), and after annealing in different environments (H_2, N_2 or FG). The spectra were baseline corrected and are vertically offset for visual clarity.

were disregarded. From CV measurements, the donor concentration, N_d, and the built-in voltage, V_0, were deduced, using the depletion approximation [59]. In order to calculate N_d, knowledge of the static relative dielectric constant for TiO_2, ϵ_{TiO_2}, is required. Here, a value of $\epsilon_{TiO_2} = 160$ at room temperature was assumed [62, 63].

3. Results and discussion

3.1. TiO_2 single crystals

N-type TiO_2 single crystals with a bluish color and conductivities in the range from $(0.5 - 8) \times 10^{-2}\ \Omega^{-1}\ cm^{-1}$ were obtained by heat-treating as-received nominally-undoped TiO_2 single crystals in forming gas flow, N_2 flow or H_2 gas. Similarly, the Nb-doped TiO_2 single crystals exhibited also *n*-type conductivity ($\sigma = 0.25\ \Omega^{-1}\ cm^{-1}$) and a dark bluish color. It is generally observed that conductive *n*-type TiO_2 single crystals display a bluish color [18, 25, 26, 65–68]. The relation between the electrical conductivity and optical absorption of the heat-treated TiO_2 single crystals is investigated further in [69].

Figure 2 displays infrared absorption spectra recorded on as-received TiO_2 single crystals (nominally undoped as well as Nb-doped) and heat-treated TiO_2 single crystals. Data are shown for the wavenumber region where optical absorption associated with a local vibrational mode of H_i can be seen [55]. From the integrated area of this line, [H_i] in the samples can be estimated [56]. Typically, nominally-undoped TiO_2 single crystals display [H_i] in the range of $10^{17}\ cm^{-3}$, while Nb-doped crystals show [H_i] below the detection limit of the measurement which is estimated to be below $1 \times 10^{15}\ cm^{-3}$. [$H_i$] of TiO_2 single crystals heat-treated in FG flux or H_2 gas increases, while TiO_2 single crystals annealed in N_2 display a decreased [H_i] concentration compared to nominally-undoped TiO_2 crystals. H_i is reported to be a shallow donor in TiO_2 [55, 70, 71], and is likely to be responsible for the conductivity observed in samples heat-treated in FG flow or H_2 gas [69]. Notably, no change in the [H_i] of the samples was observed over the course of a few months when storing the crystals at around −20 °C [69]. σ, however, decreased slightly with time. σ was measured on FG-TiO_2 crystals after annealing, and

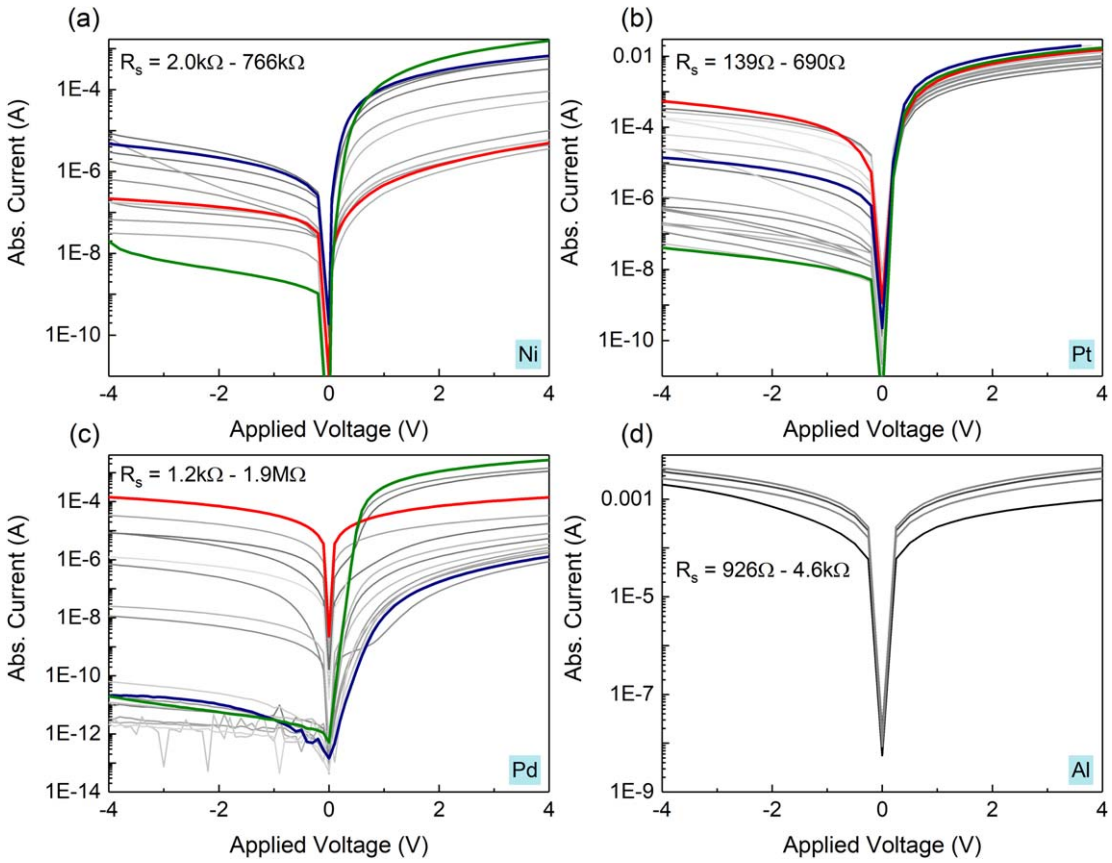

Figure 3. IV measurements recorded on different metal/TiO_2/InGa junctions comprising FZ-grown FG-TiO_2(001) crystals. Each figure (a)–(d) displays IV curves measured on all of the different SBDs fabricated using the same TiO_2 crystal (see figure 1). IV curves of the SBD with the highest rectification, the lowest rectification and medium rectification are plotted in green, red and blue, respectively.

remeasured 40 days later. These measurements showed a reduction of ∼5% in σ after 40 days of storage, which was larger than the relative standard deviation of the measurements (∼1%).

3.2. Metal/TiO_2 junctions

3.2.1. Influence of the choice of metal

Figure 3 shows IV curves recorded on junctions between FZ-grown FG-TiO_2(001) and various metals. Rectifying junctions are formed for Pd/TiO_2, Pt/TiO_2 and Ni/TiO_2, while Ohmic contacts are obtained for Al/TiO_2, as anticipated from the expected barrier heights stated in table 1. The highest rectification observed was eight orders of magnitude and was observed for Pd/TiO_2 junctions. Usually, independent of the exact annealing condition, rectifications between $2 - 5$ order of magnitude are achieved for Pd, Pt as well as Ni contacts on TiO_2. Series resistances in the order of 100 Ω to 1 MΩ were obtained. Typically, ideality factors between 1.1 and 4.0 are found. η larger than 2 can, for example, be related to the presence of a highly-compensated interfacial layer or to recombination in the depletion region [19, 59, 72].

3.2.2. Influence of surface orientation and treatment

In figure 3, one can observe a significant spread in electrical characteristics of the SBDs deposited on the same TiO_2 single crystal (see figure 1). There is a wide spread in the values for the current under reverse as well as forward bias. The differences in electrical characteristics seen for SBDs deposited on the same TiO_2 crystal originate from a spread in values of R_s, R_{sh} and η, suggesting lateral inhomogeneities over distances of around 1 mm (see figure 1). Particularly, the differences seen for η suggest significant surface inhomogeneities, e.g., due to lateral inhomogeneities in the density of interface states or the thickness of a highly-compensated interfacial layer [57, 72, 73]. The spread observed for R_s and R_{sh} could also be related to surface inhomogeneities. R_s will here mainly comprise of contributions from the bulk resistivity and the contact resistance of the Ohmic contact, and especially the resistance of the Ohmic contact could be influenced by surface inhomogeneities [57]. R_{sh} is related to leakage currents whose magnitude might, for example, be sensitive to the density of defects within the space-charge region [74]. In figure 4, the average rectification determined for metal/TiO_2 junctions is shown, fabricated using FZ-grown FG-TiO_2(001), FG-TiO_2(110) or FG-TiO_2(100) crystals, all treated in boiling H_2O_2.

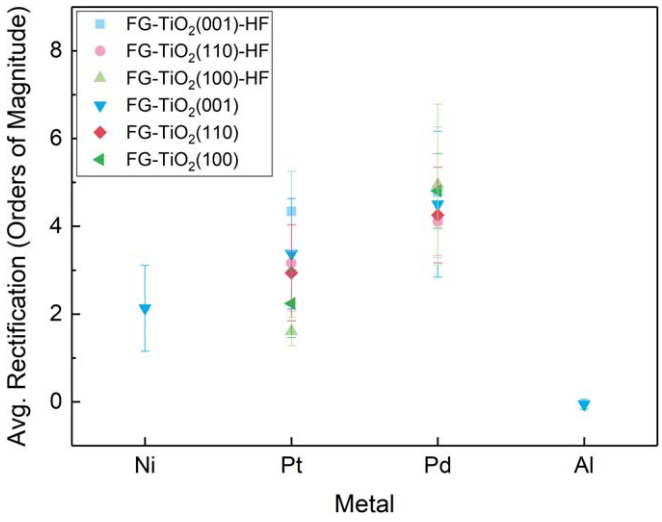

Figure 4. Average rectification determined for metal/TiO_2 junctions. For each data point, the rectifications of 15 — 20 SBDs fabricated using the same TiO_2 crystal were averaged (see figure 1). The displayed uncertainty is the standard deviation of the corresponding average.

Results are also shown for samples for which the FG-TiO_2 crystals were treated in HF prior to metal deposition (FG-TiO_2(X)-HF). The displayed uncertainty is the standard deviation determined from the averaging of the rectifications of SBDs on the same FG-TiO_2 crystal. Regardless of surface orientation, surface treatment or choice of metal, a large spread in rectification can be seen. This suggests that either the spread in rectification is related to a universal surface characteristic of TiO_2 or it is related to a bulk property. Importantly, the spread found for η and R_{sh} is most likely related to surface properties, while the spread in R_s can be related to bulk and surface properties. It has previously been found that hydroxyl layers can form on the TiO_2 surface and influence the electrical characteristics of metal/TiO_2 junctions [19]. One would, however, expect HF treatments to affect the electrical characteristics in this case. It was also found that the treatment in H_2O_2 did not have a significant effect on the quality of the SBDs (not shown). The experiments summarized in figure 4 seem to demonstrate that deposition of Pd yields the best SBDs. Therefore, Pd diodes were selected for further characterization.

3.2.3. Comparison between resistivity and SBD series resistance

Values for ρ of FZ-grown H_2-TiO_2 crystals annealed at different temperatures between 400 °C and 600 °C for durations of 10–90 min were measured prior to metal contact deposition. In figure 5, the resistivity estimated from IV measurements, ρ_{IV}, for several SBDs on each H_2-TiO_2 crystal, is plotted as a function of resistivity, ρ. As shown in the figure, the least resistive crystals have values for ρ_{IV} very close to ρ. For more resistive crystals, ρ_{IV} are larger than ρ. This result indicates that for conductive crystals, the bulk resistivity is limiting the series resistance, but for more resistive crystals, contact resistance becomes important. Moreover, this result suggests that the contact resistance is dependent on the doping concentration of the crystal. The relative deviation in ρ_{IV} between different diodes is similar for all crystals, as shown in the inset of figure 5.

3.2.4. Influence of doping

Doping levels suitable for electrical measurements were achieved by annealing in forming gas at 600 °C for ~1 h, in H_2 at 450 °C for 30–60 min, or in N_2 at 1100 °C for ~90 min. Figure 6 shows IV curves recorded on Pd/TiO_2 junctions comprising FZ-grown H_2-TiO_2(001), V-grown FG-TiO_2(001), V-grown N_2-TiO_2(001) and V-grown Nb-TiO_2(001). Rectifying junctions are obtained regardless of the doping procedure used. The resulting junctions exhibit ideality factors from 1.1 to 4, and values for the series resistance in the order of 10 Ω to 100 MΩ. A large spread in electrical characteristics is also seen for Pd/TiO_2 junctions comprising TiO_2 crystals doped using different strategies, both between the differently treated crystals, and between SBDs on the same crystal (see figure 1). In figure 6, one can observe a significant spread in the values of R_s, R_{sh} and η of the SBDs deposited on the same TiO_2 single crystal, resulting in a wide range of values for the current under reverse as well as forward bias, similar to what is seen in figure 3. Notably, Nb-doped TiO_2 displays the same spread in electrical characteristics. Thus, one can conclude that the inhomogeneity causing the large spread in electrical characteristics is not caused by heat-treating the samples in reducing or hydrogenating atmospheres. Moreover, H is not likely to play a role in the observed inhomogeneity taking into account that the Nb-doped TiO_2 crystals were shown to contain significantly less H_i than the hydrogenated or reduced TiO_2 crystals (see figure 2).

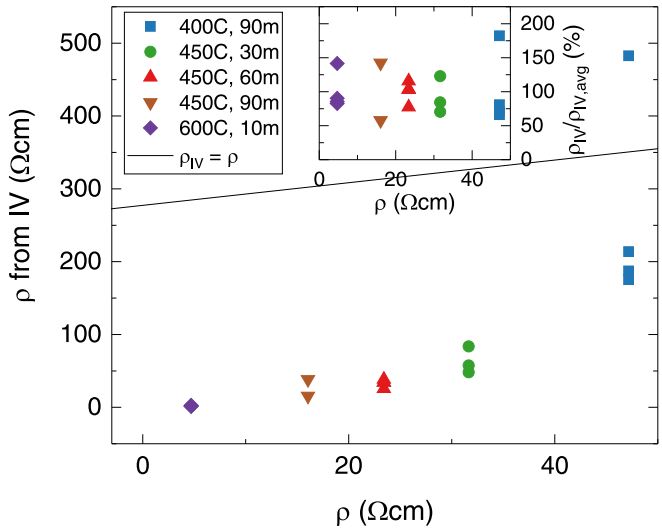

Figure 5. ρ_{IV}, extracted from IV measurements, as a function of ρ for a series of FZ-grown H_2-TiO_2 crystals annealed at temperatures from 400 °C to 600 °C for 10–90 min. The resistivity of each crystal was measured before Pd contacts were deposited. Each data point corresponds to a measurement on a single SBD.

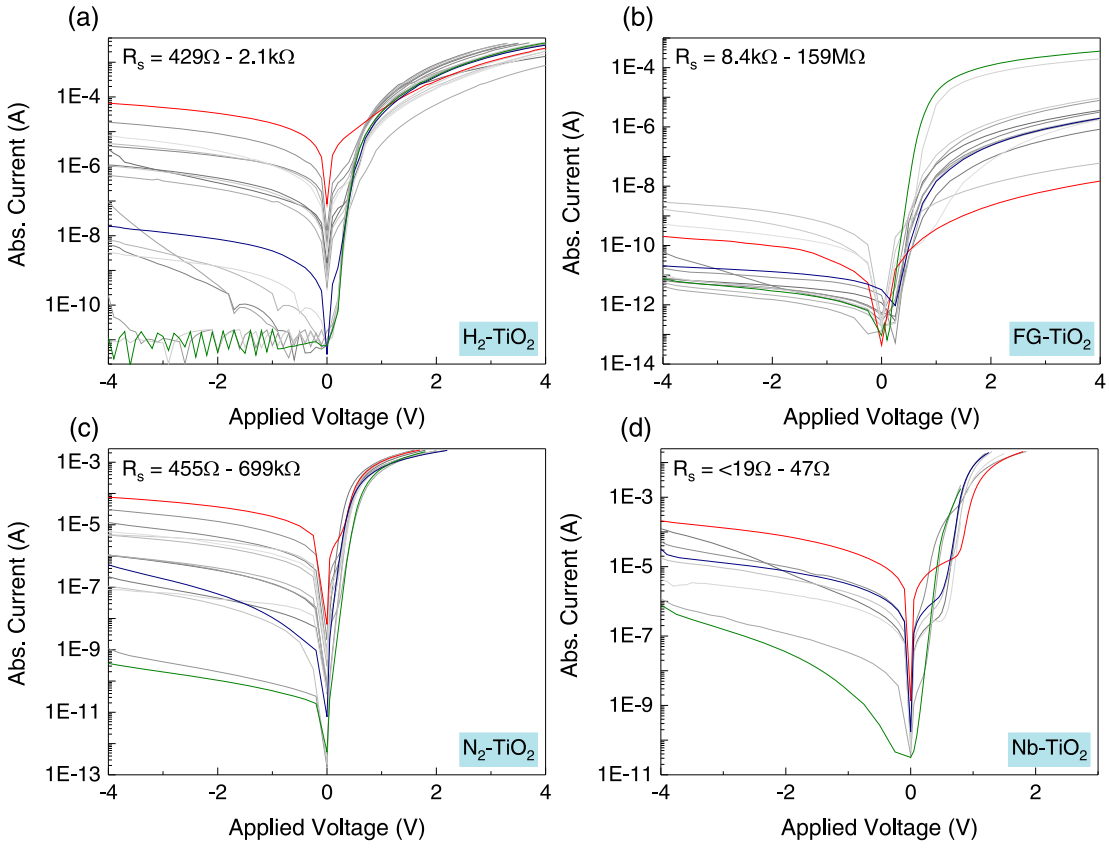

Figure 6. IV measurements recorded on Pd/TiO_2 junctions, comprising different TiO_2 crystals; (a) FZ-grown H_2-TiO_2, (b) V-grown FG-TiO_2, (c) V-grown N_2-TiO_2, and (d) V-grown Nb-TiO_2. Each figure (a)-(d) shows IV curves measured on all of the different SBDs fabricated using the same TiO_2 crystal (see figure 1). IV curves of the diode with the highest rectification, the lowest rectification and a medium rectification are plotted in green, red and blue, respectively.

3.2.5. Schottky barrier height and Built-in voltage

The determination of barrier heights from IV characteristics is only reliable if the current is determined by thermionic emission [75]. For the SBDs studied here, this is not the case, since η is larger than 1.1 at room temperature [75]. The SBDs that exhibited the lowest values of η were measured also at lower temperatures T. IV-T curves from a Pd/H_2-TiO_2 junction are plotted in figure 7(a). $\eta(T)$ displays an abnormal decrease with

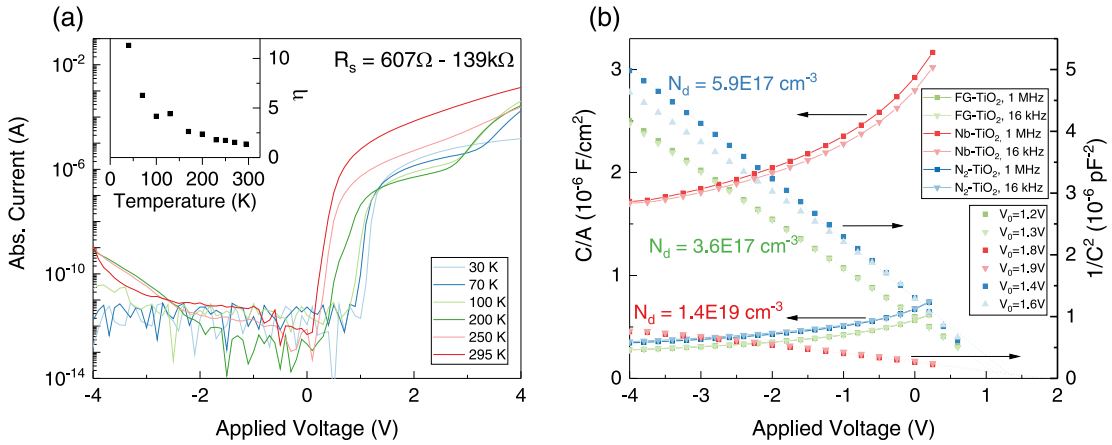

Figure 7. (a) IV measurements recorded on a Pd/H_2-TiO_2(001) junction at different temperatures between 30 K and 295 K. (b) Frequency-dependent room temperature CV measurements recorded on Pd/TiO_2 junctions, comprising different TiO_2 crystals. The crystals are FZ-grown FG-TiO_2(001) (green), FZ-grown N_2-TiO_2(001) (blue) and V-grown Nb-TiO_2(001) (red). The extracted series resistances of the crystals are 165 Ω (FG-TiO_2), 136 Ω (N_2-TiO_2) and ∼10 Ω (Nb-TiO_2).

increasing T, as shown in the inset. Such a temperature-dependence leads to a non-linear shape of the Richardson plot ln (I_0/T^2) versus $1/T$, where I_0 is the reverse saturation current [75], and the value for the effective Richardson constant A^* and Φ_B could not be extracted. A similar temperature dependence of η was found regardless of the crystal growth method, choice of metal or the doping procedure used. These measurements are in line with previously reported temperature-dependent IV data measured on Schottky junctions involving TiO_2 [44, 48, 76]. Recently, Φ_B has been deduced from IV-T data measured on junctions involving TiO_2 that display similar non-ideal behaviour [48, 76]. In [76] and [48], Φ_B was extracted assuming barrier height inhomogeneities (BHI) and using a model proposed by Werner and Güttler[77]. For the junctions studied here, however, which were measured at lower temperatures, this model can only explain the non-ideal behaviour of IV measurements recorded at T larger than ∼100 K–150 K. For $T < 100$ K, the requirement of a linear relationship between η and Φ_B, which confirms the existence of BHI [78], is not fulfilled. In addition, the modified Richardson plot provides reasonable values for A^* and Φ_B, but only in the temperature range above 100 K. Therefore, it is possible that BHI affect the current transport, but at low temperatures, other mechanisms are also important.

The built-in voltage for Pd/TiO_2 junctions was determined from CV measurements. Figure 7(b) shows results of CV measurements recorded on Pd/TiO_2 junctions comprising FZ-grown FG-TiO_2(001), V-grown N_2-TiO_2(001) and V-grown Nb-TiO_2(001) crystals. The representation of CV measurements as $1/C^2$ versus V are straight lines, suggesting a homogeneous donor concentration in the depletion region. Notably, CV measurements at different f_{meas} display a slight dispersion. V_0 was determined to be 1.2 V–1.3 V for Pd/FG-TiO_2(001), 1.4 V–1.6 V for Pd/N_2-TiO_2(001) and 1.8 V–1.9 V for Pd/Nb-TiO_2(001) junctions, depending on f_{meas}. Notably, a N_d of 1.4×10^{19} cm^{-3} was determined for the Nb-TiO_2(001) crystal, being close to the Nb concentration of 1.38×10^{19} cm^{-3} expected in these crystals according to the wt% of Nb specified by the supplier [54]. Thus, the determination of N_d from CV measurements is corroborated. The V_0 deduced is larger than expected, considering the theoretically calculated SBD heights given in table 1.

The results shown in figure 7(b) show that the fabricated Pd/TiO_2 junctions are suitable for space-charge spectroscopy techniques, such as deep-level transient spectroscopy [79] or thermal admittance spectroscopy [80], and hence the junctions can be used to study electrically-active defects in TiO_2 [41]. It is, however, important to verify the suitability of a specific junction for space-charge spectroscopy, i.e., junctions suitable for space-charge spectroscopy should display low series resistance as well as ideality factors close to 1 [57].

3.2.6. Time-evolution of electrical characteristics

Pd/TiO_2 junctions were stored at −20 °C for several months, and IV curves were recorded every few days. Most Pd/TiO_2 junctions exhibit a decrease in rectification over the course of a few weeks regardless of the doping used for the TiO_2 crystal. It has been reported previously that the electrical characteristics of rectifying metal/TiO_2 junctions change over time, and a reaction between H and Pd has been suggested to be the cause of the degradation [46, 47, 49]. Figure 8(a) displays IV curves from a Pd/TiO_2 junction recorded at different times after initial contact deposition. The junction comprises a FZ-grown FG-TiO_2(001) crystal. The series resistance and ideality factor of the Pd/TiO_2 junction do not change significantly over the course of several weeks, while the current under reverse bias notably increases, and thus the overall rectification decreases. Such a degradation was

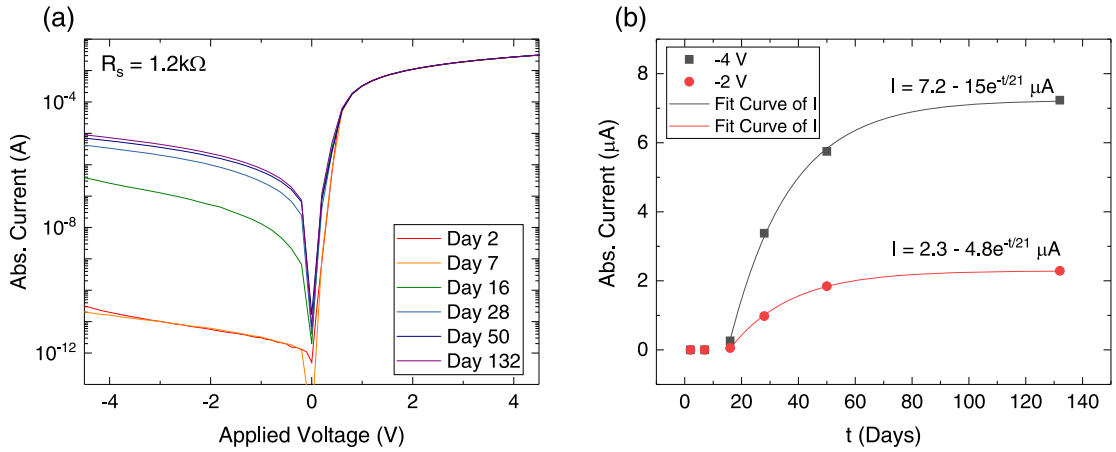

Figure 8. Example of SBD degradation illustrated by IV measurements recorded on a Pd/FG-TiO_2(001) junction over a period of 4 months. (a) IV curves recorded on different days after Pd deposition. (b) The current under reverse bias recorded at $V = -2$ V and $V = -4$ V over a period of 4 months, fitted by a function of the form $I(t) = I_0 - c_1 \exp(-t/\tau)$.

typically observed for the SBDs comprising FG-TiO_2(001) crystals. Pd/TiO_2 junctions comprising TiO_2 crystals doped using heat-treatments in H_2 or N_2 also display a similar degradation behaviour. Thus, the observed degradation is related to a decrease in shunt resistance of the Pd/TiO_2 junctions. Figure 8(b) shows the current under reverse bias as a function of time. Initially, there is very little change in the magnitude of the reverse current. After a few weeks, a pronounced increase in the current under reverse bias can be seen. We fitted this increase with a first-order kinetics expression: $I(t) = I_0 - c_1 \cdot \exp(-t/\tau)$, where t is time, I_0 and c_1 are constants that vary with applied voltage and τ is the characteristic time constant. At room temperature, the best fit was obtained for $I_0 = 2.3$ μA, $c_1 = 4.8$ μA for -2 V and $I_0 = 7.2$ μA, $c_1 = 14.7$ μA for -4 V; and $\tau = 21$ days for both -2 V and -4 V.

In FG-TiO_2, H_i is expected to be the main donor, and thus the observation regarding the series resistance is in accordance with the observation that [H_i] does not change in similarly treated samples. Interestingly, this is contrary to expectations taking the large diffusion constant for H_i in TiO_2 ($D \sim 0.2$ μm^2/hour at room temperature) into account [81].

In order to study the observed degradation further, IV curves of the Pd/TiO_2 junctions comprising a FZ-grown H_2-TiO_2(001) crystal were recorded every few days until the Pd contacts were removed after 42 days. During contact removal, some of the surface was polished off, leaving a rougher surface compared to as-received crystals. Fresh Pd contacts were deposited on the same crystal piece. The average rectification after first contact deposition was initially 5.2. Just before the contacts were removed, the average rectification had dropped to 1.8. Finally, after re-deposition of contacts, the average value increased to 3.0. This experiment demonstrates that a new annealing procedure is not required to improve the quality of the SBDs, and that the degradation is related to the interface. Interestingly, only R_{sh} changes over time, suggesting that the change at the Pd/TiO_2 interface related to the observed degradation does not affect the barrier itself. This observation may indicate that the degradation is caused by enhanced tunnelling of charge carriers through the space-charge region. The origin of such an enhanced tunnelling is, however, unclear. Studying the defects present at the Pd/TiO_2 interface using space-charge spectroscopy could help shedding light on the role of defects in TiO_2 regarding the observed leakage current [41].

3.3. Adhesion of Pd on TiO_2

In an attempt to study the interface between Pd and TiO_2, STEM was performed on a FIB sample fabricated from the edge of a Pd/TiO_2 junction, covering both the junction and plain TiO_2. Figure 9 displays a STEM micrograph recorded on a Pd/TiO_2 junction after preparing a lamella using FIB. A gap between the Pd contact and TiO_2 crystal is clearly visible. A 100 nm thick Pd layer was confirmed present by energy-dispersive x-ray spectroscopy and high-angle annular dark-field imaging. However, it was found that the adhesion of Pd on TiO_2 crystals is poor. During FIB milling, local stress relaxation or heating induced by the beam at the Pd-TiO_2 interface may have caused the Pd-film to detach. Poor Pd-adhesion was also found during fabrication of the samples: Some Pd contacts detached from the TiO_2 during cleaning in acetone and isopropanol in an ultrasonic bath.

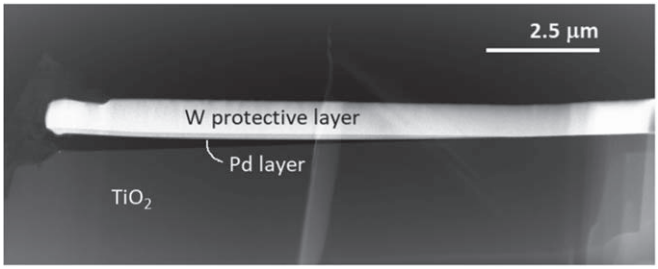

Figure 9. STEM high-angle annular dark field cross-sectional image of a Pd/TiO_2 junction.

4. Conclusion

We have studied the formation of metal/TiO_2 junctions comprising Pd, Pt, Ni and Al. For this purpose, different strategies for obtaining conductive *n*-type TiO_2 single crystals were employed. Conductive *n*-type TiO_2 with conductivities ranging from $(0.5 - 8) \times 10^{-2}\ \Omega^{-1}\ cm^{-1}$ was obtained by heat-treatments in hydrogenating or reducing atmospheres. For comparison, Nb-doped TiO_2 ($\sigma = 0.25\ \Omega^{-1}\ cm^{-1}$) was also utilized to form metal/TiO_2 junctions. Rectifying junctions are obtained for Pd/TiO_2, Pt/TiO_2 and Ni/TiO_2 regardless of the doping procedure or the surface orientation of the TiO_2 crystals, while Al forms an Ohmic contact with TiO_2. From CV measurements, the built-in voltage was deduced to be around 1.2 V–1.9 V, depending on the doping concentration of the specific TiO_2 single crystal. A large spread in electrical characteristics is found for SBDs fabricated on the same TiO_2 crystal regardless of the doping strategy or the surface orientation. Ideality factors extracted from IV measurements were in the range of $1.1 - 4.0$ at room temperature, whereas values for the series resistance range from ~10 Ω–100 MΩ. Most Pd/TiO_2 junctions exhibit a degradation over time. The degradation is related to an increase in the current under reverse bias voltage, whereas the series resistance and ideality factor stay approximately constant. The degradation can be described by first-order kinetics with a time constant of 21 days at room temperature. Adhesion between Pd and TiO_2 appears to be poor, which could be one of the reasons for the large spread in electrical characteristics of SBDs. Importantly, we demonstrated the fabrication of Pd/TiO_2 junctions which can be used to study fundamental properties of metal/TiO_2 junctions and electrically-active defects in TiO_2 using space-charge spectroscopy.

Acknowledgments

The Research Council of Norway is acknowledged for the support to the Norwegian Micro- and Nano-Fabrication Facility, NorFab, project number 245 963. Financial support by the Research Council of Norway via the EEA-JRP-RO-NO-2013-1 European Project (PERPHECT), and the Faculty of Mathematics and Natural Sciences at the University of Oslo via the strategic research initiative FOXHOUND is gratefully acknowledged. We would like to thank Dr. Athanasios Eleftherios Chatzitakis for patiently sharing his knowledge on modelling equivalent circuits on junctions involving TiO_2.

ORCID iDs

Julie Bonkerud https://orcid.org/0000-0001-8353-9842
Christian Zimmermann https://orcid.org/0000-0003-3708-6074
Lasse Vines https://orcid.org/0000-0001-5759-7192

References

[1] Nowotny M, Bak T and Nowotny J 2006 *The Journal of Physical Chemistry* B **110** 16270
[2] Vos K 1977 *J. Phys. C: Solid State Phys.* **10** 3917
[3] Vos K and Krusemeyer H 1974 *Solid State Commun.* **15** 949
[4] Pascual J, Camassel J and Mathieu H 1978 *Phys. Rev.* B **18** 5606
[5] Ni M, Leung M, Leung D and Sumathy K 2007 *Renew. Sustain. Energy Rev.* **11** 401
[6] Fujishima A, Zhang X and Tryk D 2008 *Surf. Sci. Rep.* **63** 515
[7] Carp O, Huisman C and Reller A 2004 *Prog. Solid State Chem.* **32** 33
[8] Cong Y, Zhang J, Chen F and Anpo M 2007 *J. Phys. Chem.* C **111** 6976
[9] Nitta A, Takashima M, Takase M and Ohtani B 2019 *Catal. Today* **321–322** 2
[10] Hoffmann M, Martin S, Choi W and Bahnemann D 1995 *Chem. Rev.* **95** 69

[11] Wang Z et al 2013 Adv. Funct. Mater. 23 5444
[12] Zheng Z, Huang B, Lu J, Wang Z, Qin X, Zhang X, Dai Y and Whangbo M 2012 Chem. Commun. 48 5733
[13] Atambo M O, Varsano D, Ferretti A, Ataei S S, Caldas M J, Molinari E and Selloni A 2019 Physical Review Materials 3 045401
[14] Pan X, Yang M, Fu X, Zhang N and Xu Y 2013 Nanoscale 5 3601
[15] DeFord J and Johnson O 1983 J. Appl. Phys. 54 889
[16] Kobayashi K, Takata M, Fujimura Y and Okamoto S 1986 J. Appl. Phys. 60 4191
[17] Sahasrabudhe G, Krizan J, Bergman S, Cava R and Schwartz J 2016 Chem. Mater. 28 3630
[18] Breckenridge R and Hosler W 1953 Phys. Rev. 91 793
[19] Farah M, Lapicque F and Matlosz M 1998 J. Electrochem. Soc. 145 3550
[20] Chester P and Bradhurst D 1963 Nature 199 1056
[21] Naldoni A, Allieta M, Santangelo S, Marelli M, Fabbri F, Cappelli S, Bianchi C, Psaro R and Dal Santo V 2012 JACS 134 7600
[22] Ohlsen W and Johnson O 1973 J. Appl. Phys. 44 1927
[23] Shannon R 1964 J. Appl. Phys. 35 3414
[24] Harris L and Schumacher R 1980 J. Electrochem. Soc. 127 1186
[25] Bogomolov V and Mirlin D 1968 Physica Status Solidi (b) 27 443
[26] Cronemeyer D 1959 Phys. Rev. 113 1222
[27] Lu T, Lin L, Wu S, Xu X and Cheng G 2002 Surf. Coat. Technol. 158–159 431
[28] Chen J, Lin L and Jing F 2001 J. Phys. Chem. Solids 62 1257
[29] Wu J, Lu S, Ge D, Zhang L, Chen W and Gu H 2016 RSC Adv. 6 67502
[30] Maeda K 2014 Catalysis Science & Technology 4 1949
[31] Sakthivel S, Shankar M, Palanichamy M, Arabindoo B, Bahnemann D and Murugesan V 2004 Water Res. 38 3001
[32] Joo S, Muto I and Hara N 2010 J. Electrochem. Soc. 157 J221
[33] Devi L and Kavitha R 2016 Appl. Surf. Sci. 360 601
[34] Nowotny M, Sheppard L, Bak T and Nowotny J 2008 The Journal of Physical Chemistry C 112 5275
[35] Zhang H, Ruan S, Li H, Zhang M, Lv K, Feng C and Chen W 2011 IEEE Electron Device Lett. 33 83
[36] Varghese O, Gong D, Paulose M, Ong K and Grimes C 2003 Sensors Actuators B 93 338
[37] Huang J, Kuo C, Chang W and Hou T 2010 Appl. Phys. Lett. 96 262901
[38] Shima H, Takano F, Muramatsu H, Akinaga H, Inoue I and Takagi H 2008 Appl. Phys. Lett. 92 043510
[39] Shima H, Zhong N and Akinaga H 2009 Appl. Phys. Lett. 94 082905
[40] Duckworth C, Brinkman A and Woods J 1983 Physica Status Solidi (a) 75 K99
[41] Zimmermann C, Bonkerud J, Herklotz F, Sky T, Hupfer A, Monakhov E, Svensson B and Vines L 2018 J. Appl. Phys. 123 161572
[42] Cerchez M, Langer H, El Achhab M, Heinzel T, Ostermann D, Lüder H and Degenhardt J 2013 Appl. Phys. Lett. 103 33522
[43] Schierbaum K, Kirner U, Geiger J and Göpel W 1991 Sensors and Actuators: B. Chemical 4 87
[44] Dittrich T, Zinchuk V, Skryshevskyy V, Urban I and Hilt O 2005 J. Appl. Phys. 98 104501
[45] Huber F 1968 J. Electrochem. Soc. 115 203
[46] Kobayashi H, Kishimoto K, Nakato Y and Tsubomura H 1993 Sensors and Actuators: B. Chemical 13 125
[47] Kobayashi H, Kishimoto K and Nakato Y 1994 Surf. Sci. 306 393
[48] Kumar A, Sharma K, Chand S and Kumar A 2018 Superlattices Microstruct. 122 304
[49] Yamamoto N, Tonomura S, Matsuoka T and Tsubomura H 1980 Surf. Sci. 92 400
[50] Altuntas H, Bengi A, Asar T, Aydemir U, Sarıkavak B, Ozen Y, Altındal Ş and Ozcelik S 2010 Surf. Interface Anal. 42 1257
[51] Szydlo N and Poirier R 1980 J. Appl. Phys. 51 3310
[52] Fu Q, Wagner T, Olliges S and Carstanjen H 2005 J. Phys. Chem. B 109 944
[53] Float-zone-grown r-TiO_2 from MTI Corporation, https://www.mtixtl.com/tio2substrates.aspx, accessed: 2019-12-05
[54] Verneuil-grown r-TiO_2 from Shinkosha, https://www.shinkosha.com/english/sehin/2_03.html, accessed: 2019-12-05
[55] Herklotz F, Lavrov E and Weber J 2011 Phys. Rev. B 83 235202
[56] Johnson O, DeFord J and Shaner J 1973 J. Appl. Phys. 44 3008
[57] Blood P and Orton J 1992 The Electrical Characterization of Semiconductors: Majority Carriers and Electron States Academic, Techniques of Physics vol 13 (New York: Academic)
[58] van der Pauw L 1958 Philips Tech. Rev. 20 220
[59] Rhoderick E and Williams R 1988 Metal-Semiconductor Contacts, Monographs in Electrical and Electronic Engineering (Oxford: Clarendon)
[60] Butler M and Ginley D 1978 J. Electrochem. Soc. 125 228
[61] Schroder D 2006 Semiconductor Material and Device Characterization (New York: Wiley)
[62] Bonkerud J, Zimmermann C, Weiser P, Vines L and Monakhov E 2020 Determining the dielectric constant of rutile TiO_2 from implanted H-profiles, In preparation
[63] Parker R 1961 Phys. Rev. 124 1719
[64] Michaelson H 1977 J. Appl. Phys. 48 4729
[65] Johnson O, Ohlsen W and Kingsbury P Jr 1968 Phys. Rev. 175 1102
[66] Khomenko V, Langer K, Rager H and Fett A 1998 Phys. Chem. Miner. 25 338
[67] Valigi M, Cordischi D, Minelli G, Natale P, Porta P and Keijzers C 1988 J. Solid State Chem. 77 255
[68] Porter V, White W and Roy R 1972 J. Solid State Chem. 4 250
[69] Weiser P, Zimmermann C, Bonkerud J, Vines L and Monakhov E 2020 Donors and polaronic absorption in rutile TiO_2 single crystals in preparation
[70] Weber J, Lavrov E and Herklotz F 2012 Physica B 407 1456
[71] Shimomura K, Kadono R, Koda A, Nishiyama K and Mihara M 2015 Physical Review B—Condensed Matter and Materials Physics 92 075203
[72] Card H and Rhoderick E 1971 J. Phys. D: Appl. Phys. 4 1589
[73] Parker G H and Mead C A 1969 Appl. Phys. Lett. 14 21
[74] Sathaiya D M and Karmalkar S 2006 J. Appl. Phys. 99 093701
[75] Rhoderick E 1982 IEE Proc. I: Solid State and Electron Devices 129 1
[76] Rawat G, Kumar H, Kumar Y, Kumar C, Somvanshi D and Jit S 2017 IEEE Electron Device Lett. 38 633
[77] Werner J and Güttler H 1991 J. Appl. Phys. 69 1522
[78] Tung R 1992 Phys. Rev. B 45 13509

[79] Lang D V 1974 *J. Appl. Phys.* **45** 3023
[80] Pautrat J, Katircioglu B, Magnea N, Bensahel D, Pfister J and Revoil L 1980 *Solid-State Electron.* **23** 1159
[81] Hupfer A, Monakhov E, Svensson B, chlygin I and Lavrov E 2017 *Sci. Rep.* **7** 1